Acta Crystallographica Section B
Structural
Science
ISSN 0108-7681

Structural characterization of Ni_2Si pseudoepitaxial transrotational structures on [001] Si

Alessandra Alberti,* Corrado Bongiorno, Paola Alippi, Antonino La Magna, Corrado Spinella and Emanuele Rimini

CNR-IMM, Stradale Primosole 50, 95121 Catania, Italy

Correspondence e-mail: alessandra.alberti@imm.cnr.it

Received 8 February 2006
Accepted 31 July 2006

The formation of pseudoepitaxial transrotational structures has been observed during the early stage of the reaction of thin Ni layers on [001] Si substrates. During the reaction, large Ni_2Si domains, characterized by single bending contours, establish a close relationship with the silicon lattice. The silicide domain consists of a core region, along the bending contour, where the silicide layer has grown epitaxially with silicon. Outside the core, the planes, at first parallel to the bending contour, continuously bend over the range 15–20°, whilst those at 90° remain aligned with silicon across the interface. Owing to the cylindrical symmetry of those transrotational structures, transmission electron microscopy analyses provided direct evidence of the bending phenomenon and allowed a complete description of the fully relaxed domain structure. A non-conventional mechanism of strain relaxation has been proposed, which is competitive with respect to the usual formation of misfit dislocations. The competitive phenomenon consists of Ni_2Si lattice bending and rearrangement of the interface to minimize the Gibbs free energy of the domain.

1. Introduction

Transition metal silicides, such as Fe, Co and Ni silicides, very often show peculiar thermodynamic and kinetic behaviour (Pretorius & Mayer, 1997) because of the metastability of a rich variety of different phases, which are frequently favoured by the interaction with the substrate.

More recently, detailed structural investigations on the growth of thin nickel silicide layers on [001] silicon have opened new insights into the microstructural rearrangement that occurs at the silicide/silicon interface (Detavernier *et al.*, 2003; Alberti *et al.*, 2005). The results led to a generalization of the texturing concepts beyond the familiar fibre axis and epitaxial alignment, showing that off-normal fibre texture (axiotaxy; Detavernier *et al.*, 2003) and pseudoepitaxial growth by transrotational domains (Alberti *et al.*, 2005) can be generated from the interaction between thin Ni layers and silicon.

The effort in understanding and controlling thin film structure and, possibly, its stability has a deep impact on Si-based technology. Nickel silicide formation and thermal stability have been widely studied to integrate NiSi layers on Si-device architectures. Recently, major effort has been devoted to improving the structural properties of very thin layers, a few tens of nanometres, on poly Si and (001) Si substrates, thus avoiding spiking and bridging effects to preserve the integrity of shallow junctions and contacts. It has been well documented that the structural stability of thin NiSi layers is dramatically affected by agglomeration and the phase

© 2006 International Union of Crystallography
Printed in Great Britain – all rights reserved

doi:10.1107/S0108768106029727

transition to $NiSi_2$ that leads to a very rough interface and a high silicon consumption. Moreover, silicide instability becomes particularly crucial in silicon-on-insulator (SOI) substrates due to the proximity of the buried oxide to the silicide layer (Seger *et al.*, 2005).

In general, the process window for NiSi formation and stability needs to be enlarged and several methods have been proposed in the literature, *e.g.* by using ion implantation (Choi *et al.*, 2002; Wielunski *et al.*, 1981), interlayers (Chiu *et al.*, 2004) or protecting caps (Lee *et al.*, 2003; Lee, Lee, Lei & Lee, 2005), or by adding a small amount of other atomic species to nickel (Lee *et al.*, 2004; Lee, Pey, Mangelinck, Chi & Osipowicz, 2005). Nevertheless, hole formation and phase transitions still occur at quite low temperatures (923–1123 K) and are very sensitive to the silicide thickness.

In our previous work (Alberti *et al.*, 2005), it has been shown that the growth process of very thin NiSi layers on (001) silicon can be tailored in order to improve the structure of the silicide, therefore extending the window for NiSi formation and its stability (Alberti *et al.*, 2004). The crucial node resides in the formation of NiSi transrotational structures that has allowed 14 nm-thick NiSi layers to be grown up to 1173 K by spike annealing (Alberti *et al.*, 2004).

Here we show that, before NiSi transrotational structures appear, Ni_2Si transrotational domains are formed on (001) silicon substrates. Ni_2Si transrotational domains have been observed in thin layers (10–20 nm) reacted on bulk Si and SOI substrates and their lattice structure is closely related to that of the substrate. The structural characterization of the Ni_2Si domains addresses the critical role of this phase for subsequent NiSi formation.

2. Experimental

On [001] Czochralski-Si and SOI cleaned substrates, 7 and 14 nm-thick nickel layers were deposited by sputtering at $T >$ 323 K and the resultant was subsequently annealed in a furnace at 533 K for 50 and 100 min at a pressure of 5×10^{-7} torr. The reacted samples were analysed by transmission electron microscopy (TEM) in plan-view and cross-sectional configurations, and by selected area diffraction (SAD) analyses using a Jeol JEM 2010F (200 kV) microscope, to study the stoichiometry and the structural properties of the silicide domains formed during annealing. High-resolution TEM (HRTEM) and two Bragg-condition Moirè-fringe analyses have been performed to investigate the bending phenomenon and the coherency of the silicide lattice with respect to the substrate.

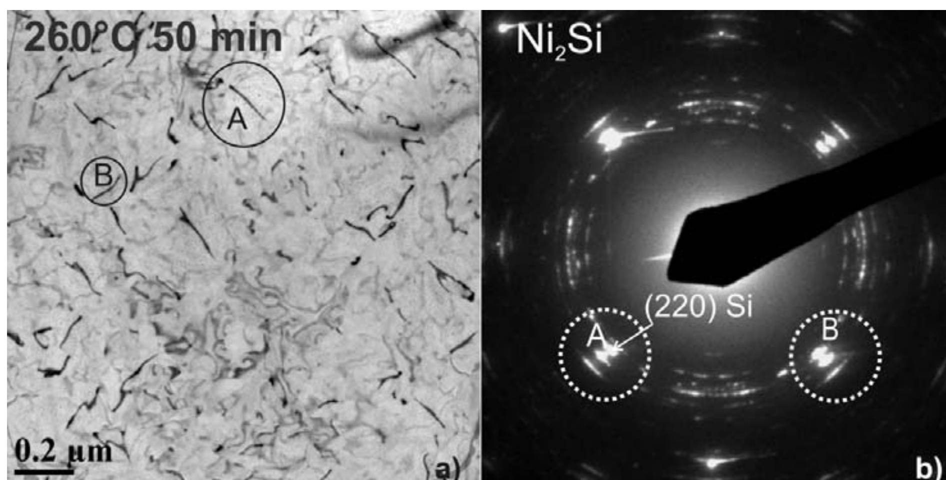

Figure 1
(*a*) Plan-view image and (*b*) the related large-area diffraction analysis of the 7 nm Ni layer after 50 min annealing at 533 K. The image and the diffraction pattern account for the formation of oriented Ni_2Si domains. In the plan-view, narrow dark lines are observed with two possible orientations that follow the symmetry of the substrate.

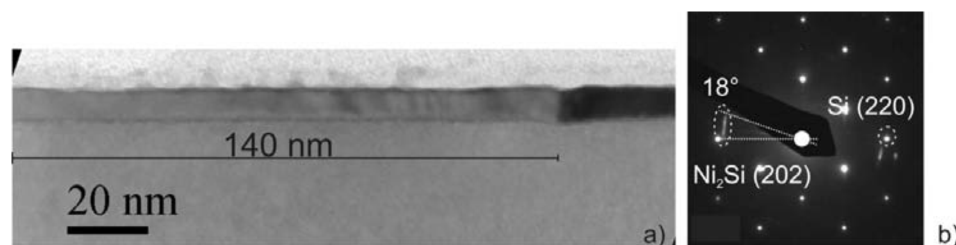

Figure 2
(*a*) Cross-sectional TEM image and (*b*) the related SAD analysis of the silicide layer. The silicide is 8.5 nm thick and has a very flat interface with silicon. The large grain on the left side of the picture produces the arc in the SAD which indicates a continuous bending of the (202) Ni_2Si planes.

3. Results

Fig. 1(*a*) shows the plan-view image of the 7 nm-thick silicide layer after annealing for 50 min at 533 K. The result is independent of the substrate. The image is characterized by an ordered distribution of narrow dark lines, each extending by a few hundred nanometres. The structure of the reacted silicide substantially differs from that of a conventional polycrystalline layer, as confirmed by the large-area diffraction pattern of Fig. 1(*b*). The pattern, which unambiguously identifies the Ni_2Si phase, is characterized by single-diffracted spots symmetrically arranged with respect to those of silicon. It has five Ni_2Si spots close to (220) Si (see dashed circles), indicating that the corresponding silicide planes, perpendicular to the sample surface, are

aligned to the silicon planes across the interface. Those five favourite planes have been identified as (203) with d = 0.1708 nm, (020) with d = 0.186 nm, (211) with d = 0.1988 nm, (202) with d = 0.2035 nm and (103) with d = 0.2121 mn. Owing to the similar d spacing, (020) and (211) planes are indistinguishable from (113) and (013) planes, respectively. All these d-spacing values roughly approach that of Si, *i.e.* d = 0.1919 nm in the range −3 to 10%. Dark-field TEM analyses have shown that the A-type oriented lines, as shown in Fig. 1(*a*), contribute in the A region of the diffraction pattern of Fig. 1(*b*). The B-type line, instead, is related to a silicide spot in the B region of Fig. 1(*b*). Following the symmetry of the substrate, only two perpendicular line orientations are therefore allowed.

A cross-sectional image of the sample is shown in Fig. 2(*a*). The silicide layer has a thickness of 8.5 nm and is characterized by quite a flat surface and a very flat interface with silicon. A portion of a large Ni_2Si grain is shown on the left-hand side of the picture. The corresponding SAD pattern, shown in Fig. 2(*b*), clearly shows the occurrence of a very peculiar relationship between film and substrate, and describes an important structural property of the grain. This peculiarity resides in the silicide grain contributing to the diffraction pattern with long arcs. They originate from the (202) planes and are characterized by an angular extension of 18°. The proximity of the arcs to the Si spots indicates that the silicide grain has a core region, where the planes are aligned to silicon across the interface. The extension of the arcs shows that, outside the core, the planes progressively bend along the entire grain section. In the direction normal to the grain section the core of the domain extends for hundreds of nanometres and generates a dark line, as shown in Fig. 1(*a*).

High-resolution analyses were carried out on the domain section to provide direct evidence of the bending phenomenon. The image was taken with a slight tilt, less than 1°, around the axis of the interface to optimize the high-resolution condition. A portion of the domain (40 nm large) is shown in Fig. 3, where (101) Ni_2Si planes join the (110) Si planes at the film/silicon interface. The silicide planes on the left side of the figure form an angle of 10°

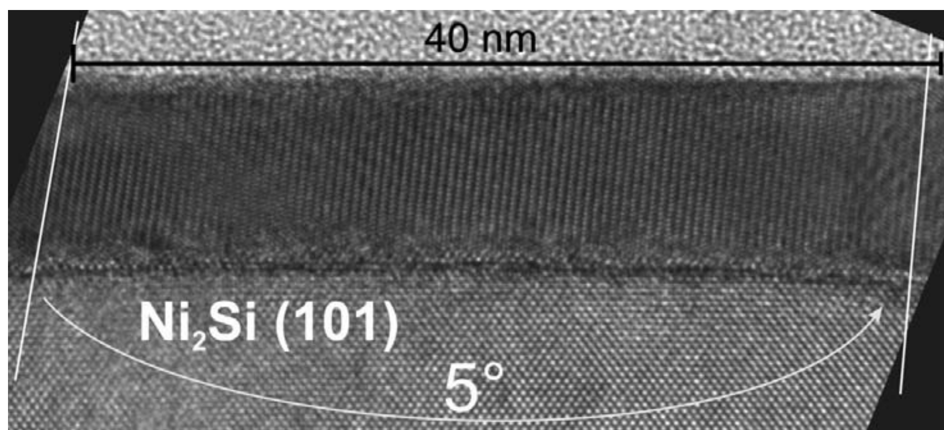

Figure 3
High-resolution TEM image of a portion of the grain shown in Fig. 2(*a*). The bending of the (101) planes is visible thanks to the cylindrical symmetry of the silicide domains.

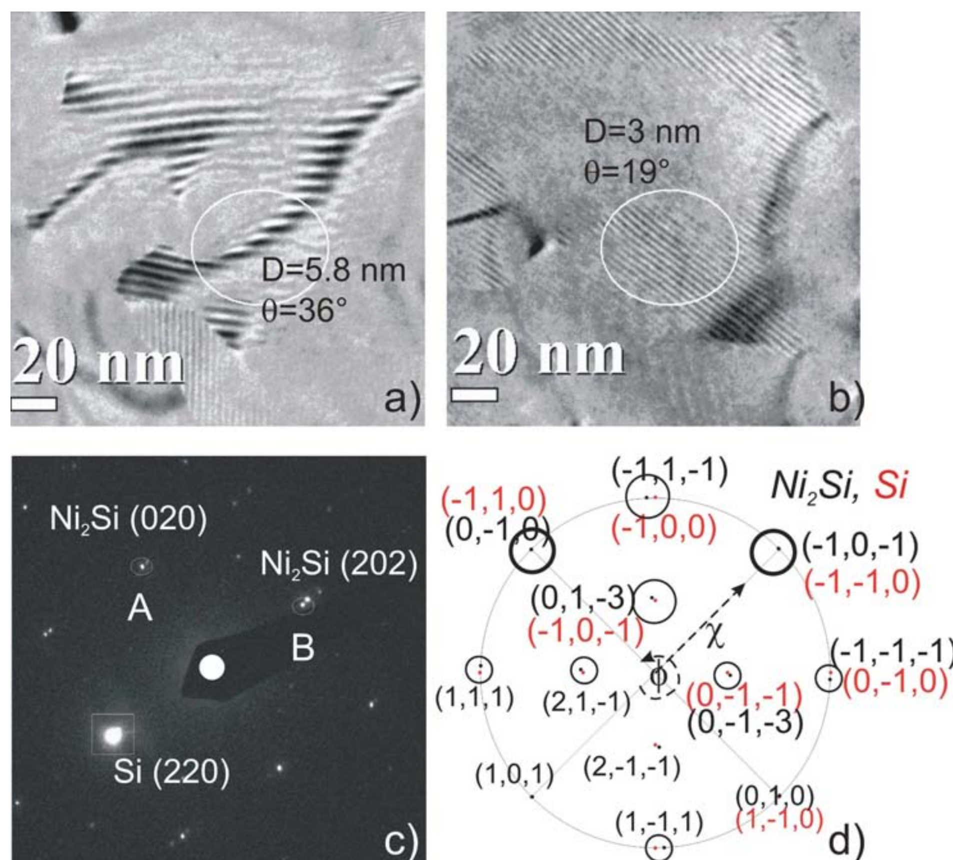

Figure 4
Moirè fringes within a Ni_2Si domain: (*a*) fringes generated by (020) planes are confined within the bending contour indicating that, outside the contour, those planes bend; (*b*) fringes generated by (202) planes are distributed all over the domain area; (*c*) plan-view SAD analysis of the domain; (*d*) three-dimensional reconstruction of the Ni_2Si lattice with respect to that of silicon.

with the direction normal to the interface. Moving to the right side, the planes progressively bend to a value of 5°, as measured at the end of the figure. The average bending rate was estimated to be as low as $0.14^\circ\ nm^{-1}$ and the interface is characterized by a narrow region, a few nm thick, where a complex microstructural rearrangement occurs. By proceeding in that direction, the core region of the domain is encountered. It has been observed that when the core extension is less than *ca* 10 nm no defects (of the dislocation type) are present at the silicide/silicon interface; otherwise misfit dislocations were formed with a density comparable to that expected by taking into account the mismatch between the planes.

The coherency of the silicide domains with respect to the substrate was studied in two Bragg conditions by using [220] Si reflections under kinematical contrast. With this method Moirè fringes were observed (Grimaldi *et al.*, 2002; Spinella *et al.*, 2000). Fig. 4 shows Moirè fringes generated by the interference of Ni_2Si planes with those of silicon within the domain region indicated by a small circle. Fig. 4(*a*) was collected by selecting the Ni_2Si spot in the A region of the selected area of Fig. 4(*c*). Additionally, the interference of the orthogonal planes (B region of the SAD) of the same domain area was selected and the resulting image is shown in Fig. 4(*b*). The two sets of Moirè fringes have different spacings (D) and orientations (θ) with respect to the generating vector of the reciprocal lattice. These values, which can be measured with high accuracy, are strictly related to the d spacing of the source planes. From the fringes of Fig. 4(*a*), values of D = 5.8 nm and θ = 36° have been measured, which give rise to the double solution of d_{max} = (0.1971 ± 0.0007) nm and d_{min} = (0.1869 ± 0.0006) nm. From Fig. 4(*b*) it has been calculated that the possible d values of the orthogonal planes are d_{max} = (0.2044 ± 0.0006 nm) and d_{min} = (0.1808 ± 0.0004) nm. The choice of the appropriate value between them is carried out by analysing the SAD pattern of Fig. 4(*c*), which indicates those planes as (020) and (202), respectively. Nevertheless, the d values measured by SAD are not as accurate as those obtained by the Moirè fringes (Grimaldi *et al.*, 2002; Spinella *et al.*, 2000). With this method of analysis it has been found that, within the core of the domain, the (020) and (202) planes of the silicide are unstrained or slightly strained by +0.5 and +0.4%, respectively. This domain structure, viewed along the [101] direction, was frequently observed over a large number of silicide domains. It is characterized by the silicide establishing a wide-ranging relationship with the silicon lattice. Besides the alignment of the (020) and (202) planes to silicon, the stereographic projection of Fig. 4(*d*) shows that the (211) and (013) planes are also very close to the (202) Si planes at χ = 45°. They have a mismatch with silicon of 3.3 and 3.6%, respectively, and differ by an azimuthal angle $\Delta\varphi \simeq 2^\circ$ and a polar angle $\Delta\chi \simeq 2^\circ$ (Fig. 4*d*). Additionally, (111) Ni_2Si planes are closely aligned to [002] Si with a mistmach as low as 1.2%, $\Delta\varphi$ = 2 and $\Delta\chi$ = 0 (see Fig. 4*d*).

The contribution of silicide domains, as shown in Fig. 4(*a*), to a plan-view large-area diffraction pattern ($2 \times 2\ \mu m^2$) is represented in Fig. 5 by the red-circled white spots. The large-area diffraction pattern was obtained by tilting the sample to reduce the substrate contributions. Simulated diffraction patterns of other domain structures have been superimposed on the same figure with different colours. It has been found that the majority of the diffraction spots arise by aligning the $(0\bar{2}0)$ silicide planes to the $(\bar{2}20)$ Si planes, as satisfied by [301] (red), [302] (blue), [202] (red-circled white) and [102] (sky-blue) oriented domains. Perpendicular to that direction, the $(10\bar{3})$, $(20\bar{3})$, $(20\bar{2})$ and $(20\bar{1})$ silicide planes are, in turn, aligned to the $(2\bar{2}0)$ silicon planes. Diffraction patterns obtained by aligning (113)//(220) were added (green spots) as significant contributions, indicating that the corresponding domains are frequently observed over a large area of the sample. With this criterion, most of the diffraction pattern was saturated (Fig. 5). The simultaneous presence of such configurations and the fact that each diffracted spot contributes to the large-area diffraction pattern with arcs (±4°) create the final pattern of Fig. 1(*b*). The arc-spots observed in the plan-view diffraction analyses have a different source with respect to the large arc of Fig. 2(*b*) (cross-sectional view), being related to a ±4° variation of the azimuthal angle (φ) describing the domain location.

4. Discussion

The structural analyses of the reacted silicide provide evidence on the formation of Ni_2Si transrotational domains. They are characterized by narrow dark lines distributed all over the sample area, having two possible orientations which follow the symmetry of the substrate. Similar diffraction contours were recently observed in 14 nm-thick NiSi layers reacted on (001) Si (Alberti *et al.*, 2005) and explained in terms of the continuous bending of the silicide lattice within each NiSi domain. In contrast to that previous result, the silicide domains shown in Fig. 1(*a*) are characterized by single bending

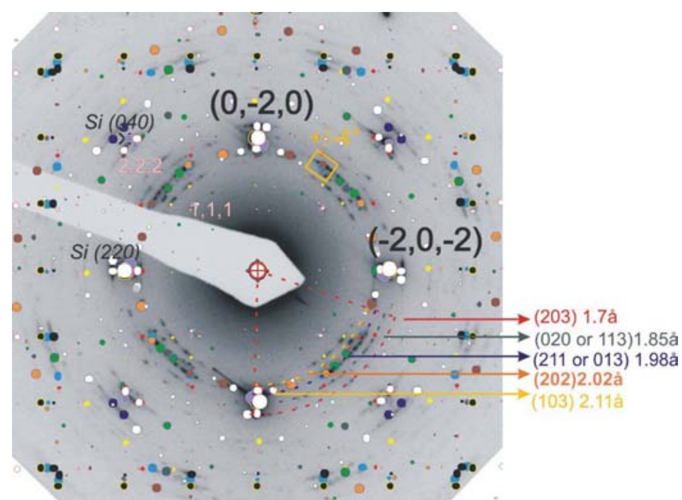

Figure 5
Plan-view large-area diffraction pattern and superimposed, simulated diffraction patterns of different domain structures indicated by spots of different colours: [301] (red), [302] (blue), [202] (red-circled white) and [102] (sky-blue) oriented domains. Perpendicular to that direction, $(10\bar{3})$, $(20\bar{3})$, $(20\bar{2})$ and $(20\bar{1})$ silicide planes are, in turn, aligned to the $(2\bar{2}0)$ silicon planes. Diffraction patterns obtained by aligning (113)//(220) were added (green spots) as significant contributions.

contours that do not cross. It has been observed (not shown) that by prolonging the annealing time to 100 min at 533 K, the single contours of Fig. 1(*a*) transform into 3–4 crossing fringes similar to those formed by 823 K spike annealing (Alberti *et al.*, 2005), and the corresponding diffraction pattern unambiguously identifies NiSi transrotational domains. Therefore, the silicide formed at the lower thermal budget (50') represents the stage of Ni reaction, characterized by the formation of Ni_2Si domains, before the transition to NiSi transrotational structures. Similar results were obtained on the 14 nm-thick Ni layer, using different annealing times (not shown).

Compared with the NiSi structures (Alberti *et al.*, 2005), the Ni_2Si domains have a cylindrical symmetry (not spherical) and are concave. This kind of symmetry allows the investigation of the bending phenomenon and the relationship between film and substrate, thanks to the fact that the e-beam integrated over the cylinder thickness preserves the information on the structural properties of the planes. Cross-sectional SAD and HRTEM analyses have shown the presence of a core region, along the bending contours, where silicide planes are aligned

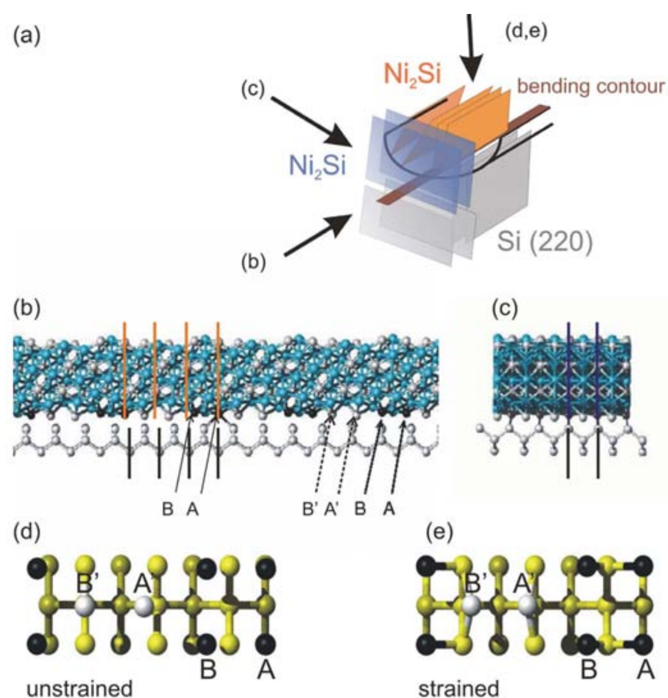

Figure 6
Ni_2Si lattice in the domain core orientation discussed in the text. Panel (*a*): schematic of the transrotational silicide domain with arrows indicating two perspective views across the interface [(*a*) and (*b*)], and top view (*c*). Panels (*b*)–(*c*): silicide and silicon lattice as viewed from (*a*) and (*b*) directions. Vertical solid lines indicate lattice plane matching between Ni_2Si(101) (orange lines), Ni_2Si(010) (blue lines) and Si(110) planes (black lines). Si atoms, *A* and *B*, at the Ni_2Si/Si interface are shown by black solid spheres. Panels (*d*)–(*e*): Si atoms in the Ni_2Si/Si interface unit cell, as viewed from (*c*), in unstrained and strained configurations, respectively. Black and white atoms are Si in the Si-terminated Ni_2Si plane, while yellow spheres are atoms of the Si substrate (the yellow scale is used to indicate the distance from the interface). Four substrate layers are drawn, following (110) silicon planes stacking (ABCD-type): the positions of the lower-most layer (dark yellow spheres) correspond to the Si(001) stacking continuation at the interface.

to those of silicon. The presence of Moirè fringes along the bending contours is an important effect of that alignment across the interface and allows accurate measurement of the interplanar distances of the planes perpendicular to the interface (Grimaldi *et al.*, 2002; Spinella *et al.*, 2000). It has been found that the core region is unstrained, and no misfit dislocations have been detected when the core width is less than ~10 nm. Outside the core, those planes progressively bend for hundreds of nanometres and lose the alignment with the substrate (Figs. 3 and 4*a*). In the region where the silicide lattice bends, the interface is usually characterized by a narrow region (1–2 nm) where a complex microstructural rearrangements occurs, and the surface region has misfit dislocations inserted from the surface to a depth of ~ 3–4 nm. The bending phenomenon does not produce layer roughening (Fig. 2*a*). In the direction perpendicular to the bending contour, the silicide planes stay vertically aligned to silicon, without bending, for the entire extension of the domain. This causes the Moirè fringes to cover the entire domain area, as shown in Fig. 4(*b*). Those planes are unstrained, and misfit dislocations were found with a density as expected on the basis of the mismatch with silicon.

The domain structure described in Fig. 4, having (020) and (202) as orthogonal planes aligned to silicon, was frequently observed. In this configuration, the silicide lattice establishes a close relationship with the substrate, as shown in the stereographic projection of Fig. 4(*c*). The stereographic projection does not take into account any lattice distortion or strain, but simply gives the impression of affinity between the two represented lattices. The proximity of the $(0\bar{1}0)$, $(\bar{1}0\bar{1})$, $(\bar{1}1\bar{1})$, $(21\bar{1})$ and $(01\bar{3})$ silicide planes to the $(\bar{1}10)$, $(\bar{1}\bar{1}0)$, $(\bar{1}00)$, (011) and $(\bar{1}0\bar{1})$ planes of Si, respectively (see Fig. 4*d*), and the similarity between the *d*-spacing values ($\Delta d/d$ in the range −3 to 6%) address the creation of a convenient interface along the bending contours. Other silicide domains, differently oriented, were found to contribute to the large area diffraction patterns of the sample, as shown in Fig. 5. However, all exhibit the common behaviour of establishing multiple relationships with the substrate. Favourable Ni_2Si planes are found close to (220)Si around χ = 45 and 90°, with φ following the symmetry of the substrate. It is found that the most part of those domains preferentially align (020) [or (113)] planes of Ni_2Si with (220) planes of Si. Those planes have the lowest mismatch with silicon.

In Fig. 6, panel (*a*), a pictorial representation of a transrotational domain with cylindrical symmetry is given: a family of silicide planes (blue) is aligned to silicon (220) ones (grey) all over the domain, while its orthogonal set of planes (orange) starts bending outside the ~ 10 nm core region (bending contour), where an unstrained and unbent silicide lattice is observed. In order to give some insight into the mechanisms responsible for the stabilization of such complex grain structures, we have built up an atomistic model of the core region, focusing on the most observed domain structure, *i.e.* that having (202) and (020) planes aligned to silicon. We discuss in the following some aspects regarding its geometry and energetics, with the aim of understanding why transrotational

domains are competitive with respect to more standard epitaxial matching.

In panels (*b*)–(*e*) of Fig. 6, the core of the domain structure is shown, from different perspectives. The silicide unit cell embedded within (010) and (101) planes is spanned by the unit-cell vectors [010] and [$\bar{1}$01] (*y* and *z* axis, in the following). The Ni_2Si [201] direction (*x* axis) forms an angle $\theta = 89.8^\circ$ with the [$\bar{1}$01] direction. Therefore, in this orientation the Ni_2Si unit cell is 'quasi'-orthorhombic. In Fig. 6, panels (*b*) and (*c*), a $(4 \times 5 \times 1)$ repetition of the (101)/(010) unstrained Ni_2Si unit cell is shown, as viewed from the *y* (left panel) and *x* directions (right panel). Vertical orange and blue lines indicate silicide (101) and (010) planes in the left and right panels, respectively. Horizontal (x,y) Ni_2Si planes containing Si atoms (white spheres) are stacked along the *z* axis with an ABC-type sequence, while layers of Ni atoms are inserted between Si-containing planes. The Si substrate lattice is also drawn, in both panels, with the Si[001] direction oriented along the vertical axis and Si(110) planes indicated by vertical black lines. In the pictures the relative position of the two semi-lattices is such that two (101) and (010) silicide planes at the center of the picture are aligned to Si(110) and Si($\bar{1}$10) planes underneath. Atomic bonds at the interface are drawn only for this set of Si atoms. Furthermore, the distance between the two interface planes, $d_{\rm int}$, is set at $d_{\rm int} = d_{\rm Si}(001) = a_0/4$ (a_0 being the bulk lattice constant of silicon).

The planar unit cell of an Si-terminated Ni_2Si interface plane is shown in panels (*d*) and (*e*) of Fig. 6. The positions of the Si atoms of the Ni_2Si (x,y) planar cell [black and white spheres, as in panel (*b*)] and those of the Si atoms in the four layers of the (3×1)-Si(001) cell underneath (yellow spheres) are shown. The silicide (x,y) unit cell is a rectangular lattice, with dimensions $l_x = l_{\rm Ni2Si}[201] = 3d_{\rm Ni2Si}(101)\sin\theta = 1.221$ nm and $l_y = l_{\rm Ni2Si}[010] = 0.372$ nm, containing four Si atoms per unit area: a pair of atoms (corresponding to black spheres *A* and *B* in Fig. 6) oriented along the [201] direction, and its twin pair (A' and B'), shifted by $\delta_x = 0.649$ nm, $\delta_y = d_{\rm Ni2Si}[010]/2$, $\delta_z = -0.03$ nm along the *x*, *y* and *z* axes. The Si(001) interface plane instead has a square pattern with sides of $d_{\rm Si}(110) = a_0/2^{1/2}$. In the figures the lattice position of atom *A* matches those of the Si(001) stacking, as in the central region of Fig. 6, panels (*b*) and (*c*), where Ni_2Si and Si planes are perfectly aligned. In panel (*d*), the interplanar distance differences between unstrained Ni_2Si and Si substrates are, as discussed above, $d_{\rm Ni2Si}(101) - d_{\rm Si}(110) = 0.022$ nm ($\varepsilon_{xx} = 0.05$), $d_{\rm Ni2Si}(010) - d_{\rm Si}(110) = -0.013$ nm ($\varepsilon_{yy} = -0.035$). In panel (*e*), the same interface structure, but with an Ni_2Si lattice strained in the *x* and *y* directions to match the Si surface dimension (*i.e.* perfect epitaxial matching), is shown.

From this geometrical model, built up from aligning a given set of planes of two unstrained bulk semi-lattices, some information on the Ni_2Si/Si interface can be extracted:

(i) Considering the planar unit cells in Figs. 6(*d*)–(*e*), it is not easy to figure out a simple rearrangement of the atomic positions of the Si atoms at the interface that may lower interface energy, in view of the different symmetry and stoichiometry of the two planar lattices [four Si atoms in the unit area of the Ni_2Si, and three atoms in the corresponding Si(001)-(3×1) area] and also of the unfavourable position of the Si-atom pair lying above Si atoms in the sub-surface layer. Large atomic relaxations can thus be expected at the Ni_2Si/Si interface (*i.e.* a 90° in-plane rotation of the unfavourable Si dimer A'–B').

(ii) In Fig. 7, a zoom-out of the core domain is shown, with lateral dimension ~ 10 nm. A long-range periodicity ($l^0 \simeq 7$ nm) along the [201] direction can be seen, corresponding to $l = 6l_{\rm Ni2Si}[201]\sin\theta = 18d_{\rm Ni2Si}(101) = 19d_{\rm Si}(110)$.

With regard to the energetics involved in the formation of grains, several contributions play a role, and increase with interface or surface area ($A_{\rm int}$, A_s) and film thickness (*h*). In general, the energy density per unit volume in a film domain, strained either uniformly (US) because of epitaxial matching with the substrate or in a continuous but not uniform way induced by plane bending (PB), can be written as $dE^{\rm xvi} = \Delta U_{\rm el}/V + (\gamma_{\rm int}A_{\rm int} + \gamma_s A_s)/V + \lambda_{\rm disl}$ (Wang *et al.*, 1999, and references therein). Here $\Delta U_{\rm el}/V$ is the elastic energy density stored, $\gamma_{\rm int}$ (γ_s) is the interface (surface) energy density per unit area and $\lambda_{\rm disl}$ is the energy density of the dislocations eventually present. Giving the theoretical estimates of all the terms above (for US and BP structures) is beyond the scope of the present work and, in general, difficult to realize with equal accuracy. Nevertheless, we discuss in the following the elastic and interface contributions, evaluated from first-prin-

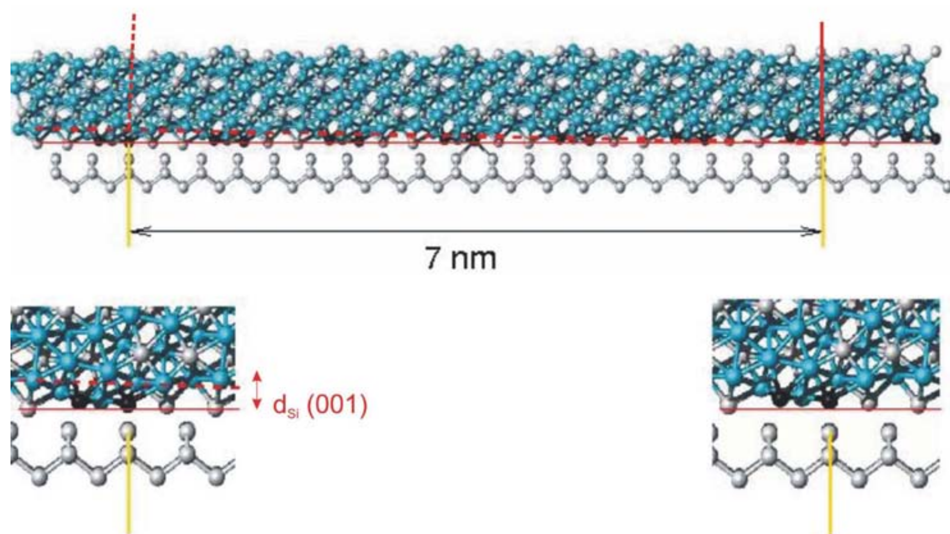

Figure 7
Ni_2Si and Si lattices in the domain core orientation, on a 10 nm length scale. The dashed red line indicates the bending of the [201] direction (see text). The zooms show that, within 7 nm, the *z* projection of the bent interface line becomes comparable to $d_{\rm Si}(001)$, also indicated for comparison.

ciple calculations from the atomistic model discussed above. In doing so we refer mostly to the energy densities per unit area, having in mind that during the specific growth process considered in the experiments the lateral dimensions of the grain increase, starting from an initial core with finite height $h = h_f$.

First we evaluate the elastic energy stored in an Ni_2Si film, (101)/(010)-oriented, uniformly strained on the interface plane to match the Si(100) lattice dimensions, *via* a set of total energy calculations for bulk Ni_2Si, in the orientation of Fig. 6. Calculations are performed within density functional theory (DFT), in the Perdew–Wang formulation of the generalized gradient approximation (Perdew, 1991) implemented in the VASP code (Kresse & Hafner, 1993, 1994; Kresse & Furthmuller, 1995, 1996). We use ultra-soft pseudopotentials (Vanderbilt, 1990) for the electron-ion interaction, a cut-off energy of E_c = 642 eV for the plane-wave expansion and a (6 × 6 × 6) Monkhorst–Pack grid for *k*-space summation. The Ni_2Si unit cell under investigation contains 36 atoms (24 Ni and 12 Si) with the vertical stacking of Ni/Si-containing layers discussed above. The theoretical equilibrium Ni_2Si lattice constants obtained with this set of cut-off parameters are $l_{VASP}[010]$ = 0.372 nm, $l_{VASP}[201]$ = 1.2207 nm, $l_{VASP}[\bar{1}01]$ = 0.8621 nm, in good agreement with experimental ones. With the [201] dimension constrained to $3d_{Ni2Si}(101)$ (*i.e.* applying planar strain $\varepsilon_{xx} = 0.05$), the total energy minimum with respect to the *y*- and *z*-axis dimensions is found at $\varepsilon_{yy} = -0.035$ and $\varepsilon_{zz} = 0.045$. From the total energy difference with the equilibrium structure we evaluate $\Delta U_{el}^{US}/V \simeq 2$ meV Å^{-3}.

In the stabilization of epitaxial films, the elastic energy stored in a volume of finite thickness, $(\Delta U_{el}^{US}/V)h$, has to be at least compensated by the gain in interface formation, γ_{int}^{US}, up to a critical thickness (surface and dislocation energies contribute as energy costs). We have calculated the Ni_2Si/Si interface energy, γ_{int}^{US}, from a supercell configuration with nine (3 × 1)Si(100) layers and five Ni_2Si layers, (101)/(010)-oriented. Owing to the periodic boundary conditions, this supercell contains two interfaces. Thus, the interface energy, calculated as half the excess energy with respect to the two bulk cells, is actually an average value. After relaxation of the atomic positions at the interface (atomic forces are < 0.01 eV Å^{-1}, in the final configuration), we obtain γ_{int}^{US} = 4.7 eV Å^{-2}. This positive (and rather large) value of γ_{int}^{US} indicates that interface formation cannot compensate the elastic energy cost, $(\Delta U_{el}^{US}/V)h$, for any value of *h*. The stabilization of ultrathin ($h \simeq 2$ nm), strained, pseudomorphic (with interface matching as in Fig. 6*e*) Ni_2Si films is ruled out from theoretical values, confirming experimental findings.

Instead, as pointed out from the geometrical analysis above, the size of long-range interface periodicity (~10 nm) shown in Fig. 7 (unstrained silicide) suggests that, for small lateral dimensions ($l < l^0$) non-pseudomorphic and non-bent regions can be stabilized, without introducing interface dislocations, assuming some interface rearrangements on the same length scale. The interface energy γ_{int}^{0} (impossible to evaluate within an atomistic framework) involves an energy cost $A^0\gamma_{int}^0$, as lateral dimensions of the grain increase.

With regard to regions where the silicide planes bend, the long-range atomic distortions involved make it impossible to evaluate the elastic energy contribution, ΔU_{el}^{BP}, within the same DFT framework as for ΔU_{el}^{US}. In any case, if it is the energetics that rule the formation of bent domains, the energy gain in the interface formation when planes bend, γ_{int}^{BP}, should be at least large enough to compensate the elastic energy density stored in a film volume with finite thickness h_f, $(\Delta U_{el}^{BP}/V)h_f$. This is not easy to justify, unless the interface energy gain, γ_{int}^{BP}, arises from some complicated interface reconstruction in the region with bent planes, on a length scale > 10 nm. Reasonably related to that, an irregular interface region is detected in the experimental TEM picture (Fig. 2). An hypothesis of such microstructural rearrangement is outlined in the following. We make use of Fig. 7 by superimposing, onto the unstrained atomic silicide lattice, two vertical lines indicating two (101) planes at a relative distance of $l \simeq 7$ nm. The left end one is rotated by *ca* 1°, *i.e.* roughly the same bending rate in the TEM picture in Fig. 2. The related continuous bending of the [201] direction is indicated by the dashed red line at the interface. As can be appreciated in the two zooms, the length of the *z* projection of the rotated interface line is close to $d_{Si}(001)$. The interface 'bending' allows, in principle, the insertion of a horizontal Si(001) plane after $l \simeq 7$ nm, *i.e.* the creation of an interface step. Such an interface rearrangement, possibly decreasing the energy cost of interface formation and taking place on a wide (>10 nm) length scale, can drive the formation of transrotational domains during growth.

To summarize, large pseudoepitaxial transrotational Ni_2Si domains have been formed at the early stage of low-temperature Ni reaction. The silicide domain consists of a core region, along the bending contour, where the silicide layer has grown epitaxially with silicon. The core usually extends less than 10 nm; it is unstrained and free of dislocations at the interface. Core regions larger than 10 nm are also observed, but in this case misfit dislocations are present according to the strain relaxation of the silicide lattice. First-principle calculations applied to the ideal case of an Ni_2Si epitaxial, pseudomorphic film indicate the large and positive interface energy as the main factor preventing the nucleation of regions with (1 × 1) interface matching and strained to exactly match the Si substrate lattice. By building up an interface atomic model on the length scale of typical core region dimensions (10 nm), we suggest that complex interface reconstructions, taking place on regions wider than the (1 × 1) area, may lower the interface energy and allow the growth of unstrained cores, as those detected in the experiments. Recent papers (Liew *et al.*, 2004; Gergaud *et al.*, 2004) have measured the strain evolution during Ni/Si solid-state reactions where different silicide phases build up between the initial [unreacted Ni/Si(001)] and final [completely reacted NiSi/Si(001)] states. A stress/strain relationship derived from elasticity theory is used to obtain values of stress at each instant of time: until Ni consumption and/or NiSi formation, Ni_2Si layers are found to grow under high compressive stress. Nevertheless, the volume expansion expected in the Ni_2Si reaction (62%) would result in a huge

planar stress at the interface, much larger than the measured values. It was indeed suggested that some fast initial relaxation mechanisms reduce part of that large stress. Although we do not explore the kinetics of the silicide growth process, our energetics arguments propose that an interfacial reconstruction occurs and has a major role in stabilizing transrotational Ni_2Si domains. Outside the core, the planes, at first parallel to the bending contour, continuously bend in the range 15–20°, with an average bending rate of $0.14^\circ\ nm^{-1}$, whilst those at 90° remain aligned to silicon across the interface. It has been observed that the planes involved in the bending phenomenon are those having a mismatch with [220] Si planes in the range −3 to 6%. The plane bending, which is concave, does not induce surface roughening and the interplanar distance measured at the surface is that of the unstrained Ni_2Si lattice. The interface with Si is, instead, modified with respect to that at the core region. The atomic model indeed offers a qualitative argument, sustaining the role of interface microstructural rearrangements on the stabilization of bent regions.

We acknowledge computational support by CINECA within a CNR–CINECA computing grant. This work was partially supported by the DD 1105 research program financed by the Italian Ministry for University and Research (MIUR).

References

Alberti, A., Bongiorno, C., Cafra, B., Mannino, G., Rimini, E., Metzger, T., Mocuta, C., Kammler, T. & Feudel, T. (2005). *Acta Cryst.* B**61**, 486–491.

Alberti, A., Cafra, B., Bongiorno, C., Mannino, G., Privitera, V., Kammler, T. & Feudel, T. (2004). *Mater. Sci. Eng. B*, **114–115**, 42–45.

Chiu, S. L., Chu, Y. C., Tsai, C. J. & Lee, H. Y. (2004). *J. Electrochem. Soc.* **151**, G452–G455.

Choi, C.-J., Ok, Y.-W., Hullavarad, S. S., Seong, T.-Y., Lee, K.-M., Lee, J.-H. & Park, Y.-J. (2002). *J. Electrochem. Soc.* **149**, G517–G521.

Detavernier, C., Özcan, A. S., Jordan-Sweet, J., Stach, E. A., Tersoff, J., Ross, F. M. & Lavoie, C. (2003). *Nature (London)*, **426**, 641–645.

Gergaud, P., Rivero, C., Gailhanou, M., Thomas, O., Froment, B. & Jaouen, H. (2004). *Mater. Sci. Eng. B*, **114–115**, 67–71.

Grimaldi, M. G., Bongiorno, C., Spinella, C., Grilli, E., Martinelli, L., Gemelli, M., Migas, D. B., Miglio, L. & Fanciulli, M. (2002). *Phys. Rev B*, **66**, 085319.

Kresse, G. & Furthmuller, J. (1995). *Comput. Mater. Sci.* **6**, 15.

Kresse, G. & Furthmuller, J. (1996). *Phys. Rev. B*, **54**, 11169.

Kresse, G. & Hafner, J. (1993). *Phys. Rev. B*, **47**, 558.

Kresse, G. & Hafner, J. (1994). *Phys. Rev. B* **49**, 14251.

Lee, P. S., Pey, K. L., Mangelinck, D., Chi, D. Z. & Osipowicz, T. (2005). *J. Electrochem. Soc.* **152**, G305–G308.

Lee, R. T. P., Chi, D. Z., Lai, M. Y., Yakovlev, N. L. & Chua, S. J. (2004). *J. Electrochem. Soc.* **151**, G642–G647.

Lee, T. L., Lee, M. Z., Lei, T. F. & Lee, C. L. (2005). *J. Electrochem. Soc.* **152**, G158–G162.

Lee, T. L., Lee, J. W., Lee, M. C., Lee, T. F. & Lee, C. L. (2003). *Electrochem. Solid-State Lett.* **6**, G66.

Liew, K. L., Bernstein, R. A. & Thompson, C. V. (2004). *J. Mater. Res.* **19**, 676.

Perdew, J. P. (1991). *Electronic Structure of Solids* '91, edited by P. Ziesche & H. Eschrig, p. 11. Berlin: Akademie-Verlag.

Pretorius, R. & Mayer, J. W. (1997). *J. Appl. Phys.* **81**, 2448–2450.

Seger, J., Hellström, P.-E., Lu, J., Malm, B. G., von Haartman, M., Östling, M. & Zhang, S.-L. (2005). *Appl. Phys. Lett.* **86**, 253–507.

Spinella, C., Coffa, S., Bongiorno, C., Pannitteri, S. & Grimaldi, M. G. (2000). *Appl. Phys. Lett.* **76,** 173.

Vanderbilt, D. (1990). *Phys. Rev. B*, **40**, 7892.

Wang, L. G., Kratzer, P., Scheffler, M. & Moll, N. (1999). *Phys. Rev. Lett.* **82**, 4042.

Wielunski, L., Scott, D. M., Nicolet, M. A. & von Seefeld, H. (1981). *Appl. Phys. Lett.* **38**, 106–108.